Using airborne LiDAR to map forest microclimate temperature buffering or amplification

Eva Gril (a*), Marianne Laslier (a), Emilie Gallet-Moron (a), Sylvie Durrieu (b), Fabien Spicher (a), Vincent Le Roux (a), Boris Brasseur (a), Stef Haesen (c), Koenraad Van Meerbeek (c), Guillaume Decocq (a), Ronan Marrec (a), Jonathan Lenoir (a)

(a) UMR CNRS 7058 “Ecologie et Dynamique des Systèmes Anthropisés” (EDYSAN), Université de Picardie Jules Verne, 1 rue des Louvels, 80000 Amiens, France

(b) UMR Territoires, Environnement, Télédétection et Information Spatiale (TETIS), INRAE, AgroParisTech, CIRAD, CNRS, Univ Montpellier, 500 Rue Jean-François Breton 34196 Montpellier, France

(c) Department of Earth and Environmental Sciences, KU Leuven, Leuven, Belgium

*Corresponding author: gril.eva@free.fr; eva.gril@u-picardie.fr

Highlights

- Airborne LiDAR is ideal to predict forest thermal environment at a high resolution
- We used Maximum height, Plant Area & Vertical Complexity Index as structure metrics
- Forest structure explained 91 % of microclimate variability at a 10-m resolution
- We mapped the buffering or amplification effect of forest on microclimate temperature
- Ecologists, conservationists and forest managers would highly benefit from such maps

Abstract

Mapping the microclimate effect of forest canopies on understory temperature requires spatially explicit predictors at very fine spatial resolutions. Light Detection And Ranging (LiDAR) offers promising prospects in that regard, as it allows capturing the vertical dimension of vegetation structure at a very high resolution over large areas.

To explore the potential of airborne LiDAR-derived metrics to predict understory temperature, we focused on the forest of Blois (France), a 2740-ha lowland managed forest dominated by oak (*Quercus petraea*). We installed HOBO sensors measuring microclimate air temperature at one-metre height in 53 stands of contrasting vegetation structure, from open to very dense and from young regeneration to mature stages. Using a nearby weather station as the macroclimate temperature reference, we calculated the slope (log scale)

coefficient of the linear regression between microclimate and macroclimate, as a simple parameter describing the microclimatic buffering (log(slope) < 0) or amplification (log(slope) > 0) capacity of the habitat.

An airborne LiDAR flight was conducted during summer 2021, matching the timing of our temperature measurements. From the resulting 3D point cloud, three complementary metrics of forest structure were derived: the maximum height, the Plant Area Index and the Vertical Complexity Index. They were calculated for circular buffers of different radii (1 m to 100 m) centred on each HOBO sensor.

We found that the 5-m radius combining the three metrics into a single multivariate model explained the greatest proportion of variance in the microclimate effect of each stand (R^2 = 0.91). We mapped the buffering or amplification effect of vegetation structure on understory temperatures over the entire forest of Blois at a 10-m resolution. 91.4 % of the surface of the forest was significantly buffered relative to macroclimate temperature, while 2.7 % was amplified, especially in road verges, clear-cut and regeneration areas. Based on our simple linear model, we were able to derive understory air temperature maps for any temporal resolution (i.e. hourly, daily, or seasonal). The results highlight the great capacity of airborne LiDAR to retrieve forest structure parameters and generate high-resolution maps of the thermal environment.

Applications for mapping the buffering or amplification of microclimate temperature are plentiful, especially in the context of climate change. They include improving the understanding of physiological processes such as thermoregulation or phenology, modelling the thermal connectivity of the landscape, improving species redistribution models, spotting microrefugia for conservation, informing forest management for tree regeneration or

wildfire control, or even prioritising cooling recreational areas for humans to escape heatwaves in urban forests.

Graphical abstract

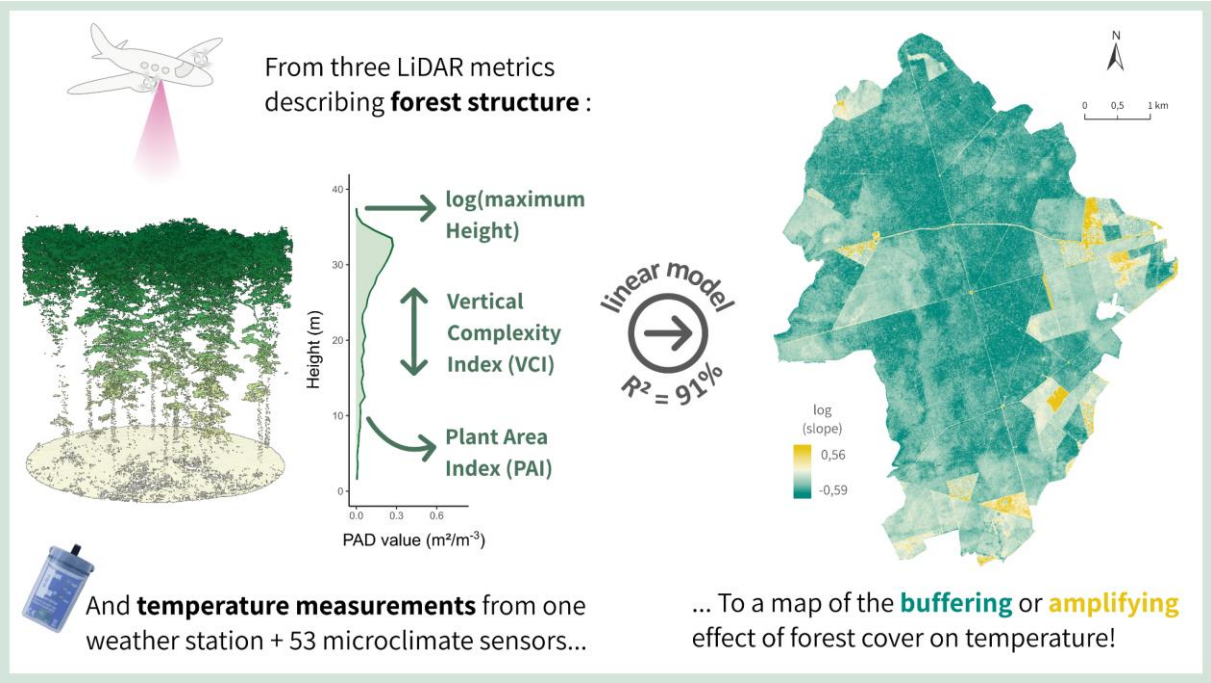

Key-Words

amplification; buffering; forest structure; forest management; airborne LiDAR; ALS; canopy height; leaf area index; microclimate; open areas; plant area index; regeneration; resolution; slope and equilibrium; temperature extremes; understory; urban forest; vegetation layers; vertical complexity index; weather station

1. Introduction

To investigate current and future impacts of temperature on species' fitness, survival or distribution, ecologists often rely on available gridded macroclimate data, with a coarse spatial resolution of 1 km² or more. This contrasts with an organism-relevant scale, where depending on their body size and physiology, species respond to variations in microclimatic temperatures at a resolution of centimetres to a few metres (Bramer et al., 2018). Another major issue is that macroclimate data is interpolated from weather stations, which are always located in open areas, exposed to sunshine and dominant winds and away from the shade of trees for the sake of standardisation (De Frenne and Verheyen, 2016). Below forest canopies, the difference between macroclimate and the local microclimate temperature is especially significant (Geiger et al., 2003). In the understory, species usually experience a buffered microclimate, with higher minimum and lower maximum air temperatures, as vegetation moderates extreme temperatures through mechanisms such as transpiration and shading (De Frenne et al., 2021). However, temperatures can instead be amplified near the ground in open or sparse vegetation (Gril et al., 2023; Pincebourde and Suppo, 2016; von Arx et al., 2013). This is especially true when airflow is reduced by trees, causing a reduction in thermal mixing alongside typical absorption of radiation, which may not be fully compensated by transpiration when vegetation is sparse, e.g. within an intraforest clearing, meadows, or under very low or sparse canopies, where lower minima and higher maxima are usually recorded for temperature compared to free-air weather station records.

These buffering or amplification effects can be highly heterogeneous, depending on local parameters such as vegetation structure. In managed forests under regular forestry, this results in diverse conditions of microclimate across small areas (Chen et al., 1999). To

effectively quantify this fine-scale thermal heterogeneity, we need spatially explicit models of temperature at fine spatial resolutions and across large spatial extents (Milling et al., 2018; Zellweger et al., 2019b).

Recent efforts have been made to obtain and gather global microclimatic data, with the goal to downscale temperature grids and get closer to conditions experienced by most terrestrial organisms (Lembrechts et al., 2020). Field-acquired dendrometric data from forest inventories are good predictors of the microclimate effect in forests (Zellweger et al., 2019a), but they are measured pointwise, and are thus inadequate for continuous mapping over a whole landscape. Using remote sensing data to upscale field measurements could help in tackling this challenge. Well-chosen remote sensing-based predictors may also have an equal, or even higher capacity than traditional field-measured variables to explain the variability in microclimate air temperature (Greiser et al., 2018; Kašpar et al., 2021). For instance, predictors acquired by satellites such as digital elevation models or the Normalised Difference Vegetation Index (NDVI) have wide coverage and have been used to generate maps of understory temperature over Europe at a 25-m resolution (Haesen et al., 2021).

The use of detailed environmental descriptors may be relevant – if not necessary – for land use planning, biodiversity conservation, better informed species distribution models, or for informing forestry management (Lenoir et al., 2017; Haesen et al., 2023; Randin et al., 2020; Zellweger et al., 2019b). Airborne thermal imaging brings interesting perspectives in that regard (Hoffrén and García, 2023), but it can only record canopy temperature, not understory temperatures near the ground – where most of the biodiversity lives in temperate forests (Gilliam, 2007). While the vertical structure of the vegetation is not well captured by satellite or airborne multispectral imagery, airborne Light Detection And

Ranging (LiDAR) allows the user to access the whole vertical structure hidden below the tree crown, including the understory shrub layer in forests, an important microclimate driver often neglected in microclimate modelling (Kovács et al., 2017; Stickley and Fraterrigo, 2021). LiDAR is the perfect tool to describe the fine-scale 3-dimensional (3D) structure of a forest and has been used for this purpose for decades (Davis et al., 2019; Lim et al., 2003; Nelson et al., 1984; Moudrý et al., 2022; Zellweger et al., 2019b). LiDAR is thus most appropriate to map microclimate processes under tree crowns (Frey et al., 2016; George et al., 2015; Greiser et al., 2018; Jucker et al., 2018).

From airborne LiDAR point clouds, we can quantify three components of vegetation structure, especially relevant in forest ecosystems: height, plant area index and vertical complexity. Tall, structurally complex forests with a large amount of vegetation are expected to be the most thermally buffered relative to macroclimate (Frey et al., 2016; Jucker et al., 2018). After creating a canopy height model from top vegetation points extracted from the 3D point cloud, maximum height can easily be mapped (Jucker et al., 2018; van Leeuwen and Nieuwenhuis, 2010).

Leaf Area Density profiles – or, more accurately, Plant Area Density profiles, given that it is difficult to separate leaves from other plant material – can be assessed from LiDAR point clouds (Bouvier et al., 2015). From these profiles, Plant Area Index (PAI) can be computed (Lenoir et al., 2022). PAI represents the cumulative area of biotic tissue per unit ground area and is related to Leaf Area Index (LAI), a key parameter for modelling exchanges (water, carbon and radiation and heat energy) between the biosphere and the atmosphere (Yang et al., 2019) which is acknowledged to have strong influence on understorey microclimate (De Frenne et al., 136 2021).

Vegetation structural complexity is the third important morphological component of an ecosystem (Valbuena et al., 2020), and can be summarised by the Vertical Complexity Index (VCI), which quantifies the "evenness" of plant material distribution, i.e. whether vegetation is clustered into layers – VCI close to 0 – or distributed evenly – VCI close to 1 – along the vertical profile (van Ewijk et al., 2011).

Here, we propose a method to map microclimate temperature in forest ecosystems, based on simple linear models and three integrative predictors of forest structure derived from airborne LiDAR. We focus on a managed forest with little to no variation in topography and with a homogenous composition in terms of the dominant tree species, but very diverse stand structures.

Our goal was to quantify the buffering or amplification effect of the forest matrix on understory air temperature, and to find the spatial scale at which these opposing processes operate. Instead of mapping microclimate temperature directly on the relevant time step (e.g. hourly, weekly or monthly), we used a novel approach to map a summary metric representing the impact on the microclimate generated by vegetation structure (i.e. the buffering or amplification capacity, Fig. 1; Gril et al., 2023). From this metric, any point-in-time or summary statistic of microclimate temperature can easily be calculated. We investigated the best scale of effect of our three LiDAR predictors, and mapped the fine-scale thermal environment of the forest at this optimal resolution.

2. Material and methods

2.1. Study area and sampling design

The forest of Blois is a 2,749-ha block of forest, with little modification of its geographical delimitation since the fifteenth century, being part of the royal, then state's domain. It is a lowland temperate forest dominated by *Quercus petraea* (sessile oak), with *Carpinus betulus* (hornbeam), *Ilex aquifolium* (holly) and *Fagus sylvatica* (beech) in the understory. The forest is managed by the French national forest office (ONF) as a regular "high forest". It is subjected to a degraded oceanic climate (Joly et al., 2010), with a mean annual temperature of 11.3°C (absolute minimum - 12°C, absolute maximum 40.1°C) and annual precipitation of 744 mm over the 1996-2004 period (ONF data). The elevation ranges from 94 to 141 m, with limited topographic variation. Soils are poor and acidic. To study a gradient of forest structure, we established 53 plots throughout the forest (Fig. 2) in diverse stages of forest management: seed trees, thicket, saplings, poles, young, adult, or mature stands.

2.2. Data acquisition

2.2.1. Microclimate and macroclimate temperature measurements

We measured hourly microclimate temperatures with commonly used sensors (Bramer et al., 2018), Onset® HOBO® Pendant data loggers UA-001-64, which have a manufacturer-reported accuracy of ± 0.53°C from 0° to 50°C, and resolution of 0.14°C at 25°C. One sensor was placed at the centre of each plot, and localized with a Trimble Geo 7X Differential Global

Positioning System, with a precision of 50 centimetres in open areas but lower (up to about 2 metres) under a dense canopy. Sensors were set up at 1-m height above the ground surface on the northside of a tree trunk (George et al., 2015). To prevent overheating due to the exposure to direct solar radiation, sensors were hung by a hook inside homemade white shields shaped like caps to ensure that there is sufficient shade and airflow at the sensor level (Gril et al., 2023; Zellweger et al., 2019a), made out of a 15-cm long, 10-cm wide PVC tube (See Fig. S0). Hourly macroclimate temperatures were recorded from a weather station located in a grassland outside but close to the forest (Fig. 2). The macroclimate sensor was shielded and placed at 1.5-m high, a common height for standardised weather stations, typically within 1.2 to 2 m above ground. Because of the deciduous canopy and because it is the most crucial period for plants and many organisms, we focused on the leaf-on period, from the beginning of June 2021 to the end of September 2021, representing a total of 155,018 hourly microclimate temperature measurements across our 53 plots.

2.2.2. Airborne LiDAR data

High-density LiDAR data were acquired by the private company ALTOA (http://www.altoa.fr/) on the 17th of June 2021, which is also why we focused this study on the leaf-on period. The LiDAR sensor used was a RIEGLVQ780-I mounted on a Partenavia P68 Observer Islander. Flight and sensor specifications are described in Table 1. Pre-processing steps such as point cloud filtering, classification (vegetation, soil, other) and point normalisation according to soil surface elevation were also performed by ALTOA. We removed points located in artificial surfaces such as buildings according to the national layer

BD TOPO® (provided by the National Institute of Geographic and Forest Information, IGN 2021, v. 3_0), plus a 1-m buffer around these polygons.

Table 1: Characteristics of the LiDAR sensor and flight

Flight Altitude	900 m
Wavelength	NIR
Pulse frequency	2000 kHz
Mean total point density	72.6 pts/m²
Mean ground points density	9.7 pts/m²
Overlap between flight lines	60 %
Scan angle	+/- 30°
Precision (Z)	4.5 cm
Geolocation error (XY)	< 0.1 m
Diameter of the spot on the ground	16.7 cm

2.3. Data processing

2.3.1. Computing the buffering or amplification capacity

Recent studies have introduced a new conceptual model linking microclimate temperature to macroclimate temperature (De Frenne et al., 2021; Gril et al., 2023). The model, validated in a wide range of temperate forest environments, uses a simple linear relationship and requires only two parameters: the slope and the equilibrium. The slope of the linear relationship between microclimate and macroclimate describes the buffering (< 1) or

amplification (> 1) capacity of the habitat (Fig. 1) and was found to be dependent on the surrounding vegetation. With a log-transformation of the slope, a value of 0 means a neutral effect of forest on temperature, while negative and positive values indicate buffering and amplification, respectively. We used a log-transformation for two reasons: first, it is easier to understand the meaning of the microclimate effect if the variable is centred on zero, where zero means a neutral effect. And second, this allows for log-log relationships in the subsequent modelling, in case a variable has a non-linear effect. The slope parameter or its log-transformation can be modelled with the usual drivers of microclimate, including forest structure metrics (Gril et al., 2023).

As for the equilibrium, it is the temperature at which microclimate equals macroclimate, i.e. the point where the identity line (Y = X) crosses the regression line of the linear relationship between microclimate and macroclimate (Fig. 1, Appendix 1). Unlike the y-intercept of a regression, it has a biophysical meaning. During sunny days, large incoming radiative fluxes exacerbate the difference between microclimate and macroclimate temperatures in forests. On the opposite, in case of wet, cloudy days with low radiative fluxes, a mild temperature is expected inside and outside the forest, leading to this situation of “equilibrium”. Therefore, the equilibrium can be approximated by the mean macroclimate temperature. Within a given season and small region, like the forest of Blois, it can be considered constant and independent from forest structure (Gril et al., 2023). We verified this independence by calculating the correlation coefficients and R^2 of linear models relating equilibrium temperatures to forest structure metrics (Appendix 2).

With both the slope and the equilibrium, the intercept can be deduced (see Appendix 1 for a demonstration), and therefore we have the complete linear relationship between microclimate and macroclimate.

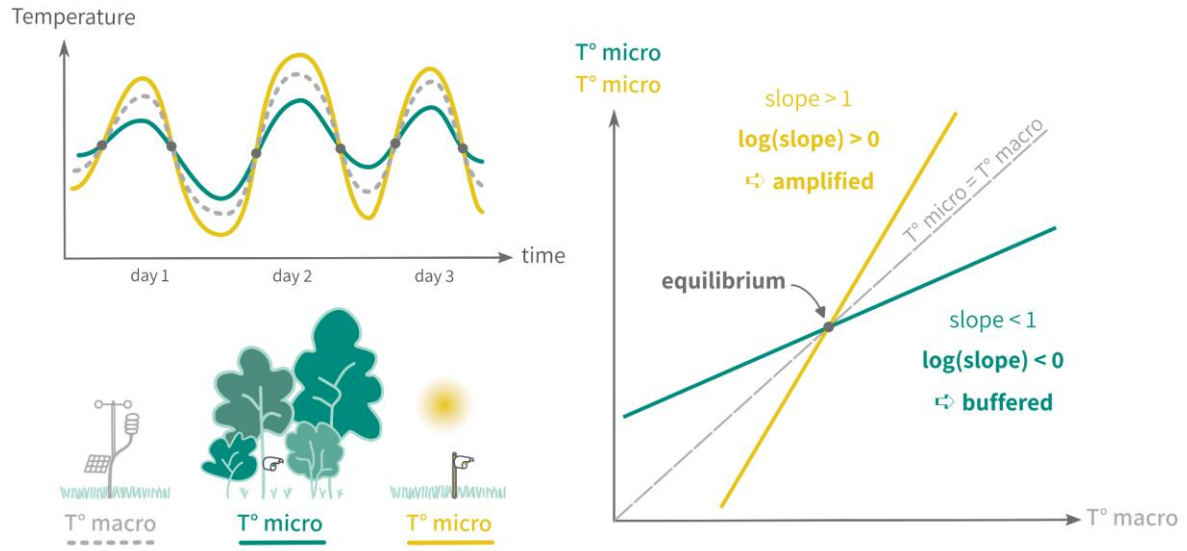

Fig. 1. The concept of the slope and equilibrium approach: two simple parameters summarising the linear relationship between microclimate and macroclimate. The slope of the linear regression describes how microclimate temperature is either buffered (e.g. under well-closed forest cover) or amplified (e.g. above the grass in an open meadow), relative to macroclimate temperature, as measured by a standardised weather station. The slope will be lower than one if temperature is buffered, and higher than one if temperature is amplified in the habitat of interest, and therefore the log-transformation of the slope parameter will respectively be lower or higher than zero. The equilibrium is the temperature for which the regression line crosses the identity line, where microclimate equals macroclimate. It is considered constant in a given site and season. For instance, if the forest

and grassland depicted here are close to one another and have the same macroclimate, then the equilibrium temperature should be considered relatively similar in both habitats.

We used the method described by Gril et al. (2023) to calculate the slope and equilibrium. We fitted a separate linear model for each of the 53 sensors, linking hourly temperature records during the leaf-on period from a given HOBO sensor to the matching hourly temperatures measured by the nearby weather station, representing macroclimate. We visually checked linearity, and computed the R squared of the regressions. In order to verify that the relationship between microclimate and macroclimate was indeed linear in this study, we compared the fit of linear models to the fit of non-linear generalized additive models (GAMs). The slope and equilibrium parameters were extracted from each linear regression, using the following equation for the latter: equilibrium = intercept / (1 - slope). Finally, we used the log of the slope as our response variable in subsequent analyses.

All analyses were performed in R version 4.1.2 (2021). We used the {tidyverse} and {lubridate} packages (Grolemund and Wickham, 2011; Wickham et al., 2019) to handle data preparation and visualisation, and {mgcv} to fit GAMs.

2.3.2. Forest structure predictors based on LiDAR data

On each of the 53 plots, we used the {lidR} package (Roussel et al., 2020) to retrieve structural metrics in different buffer sizes around the location of our microclimate sensors, ranging from a 1-m to a 100-m radius. Forest structure metrics may indeed differ in the optimal resolution used to infer them from LiDAR data (Atkins et al., 2023). We calculated

three metrics from these 3D point clouds: maximum height, Plant Area index (PAI) and Vertical Complexity Index (VCI). Note that the {lidR} package has predefined functions to compute the maximum height and the VCI, whereas users have to sum Plant Area Density (PAD) values along the vertical profile (using the *LAD* function) post hoc to acquire PAI. These three metrics give complementary information on the structure of the forest: the height, density, and distribution of vegetation along the vertical profile.

The maximum height was calculated as the highest vegetation point in a given buffer area, and was log-transformed to account for non-linear effects (Jucker et al., 2018). Hereafter we refer to this predictor variable as log(Hmax). Canopy height is well captured by airborne LiDAR, although the combination of a thick understory layer and low point density may lead to an underestimation of the height due to the understory mistakenly being considered as ground. Here, this issue is minimised since we had a very high point density (70 pts/m² on average) so that the mean density of points reaching the ground surface was approximately 10 points per square metre, even though the flight was during leaf-on conditions (Table 1).

The PAI is an estimation of the total plant area (leaves and woody structures) per unit ground surface area participating in light occlusion, and is based on the Beer-Lambert Law considering that light pulses will be attenuated through canopy cover (Vincent et al., 2015; Lenoir et al., 2022). It represents the integral, or area under the curve of the Plant Area Density (PAD) profiles, and is calculated as the sum of PAD in each vertical “vegetation slice”. Here, 1-m slices were used starting from 1.5 m height above the ground up to a maximum of 40.5 m for the highest slice that contained the maximum canopy height observed across the state forest of Blois.

Finally, the VCI quantifies the vertical layering of the vegetation (van Ewijk et al., 2011). It is a fixed normalisation of the Shannon Index, bounded between 0 and 1, with values close to 0 indicating a very uneven distribution of vegetation points (i.e. most vegetation points are located at the same height, within a single layer), while values close to 1 indicate a very even distribution of vegetation points throughout the profile (i.e. most height bins have an equal amount of vegetation, suggesting many overlapping layers).

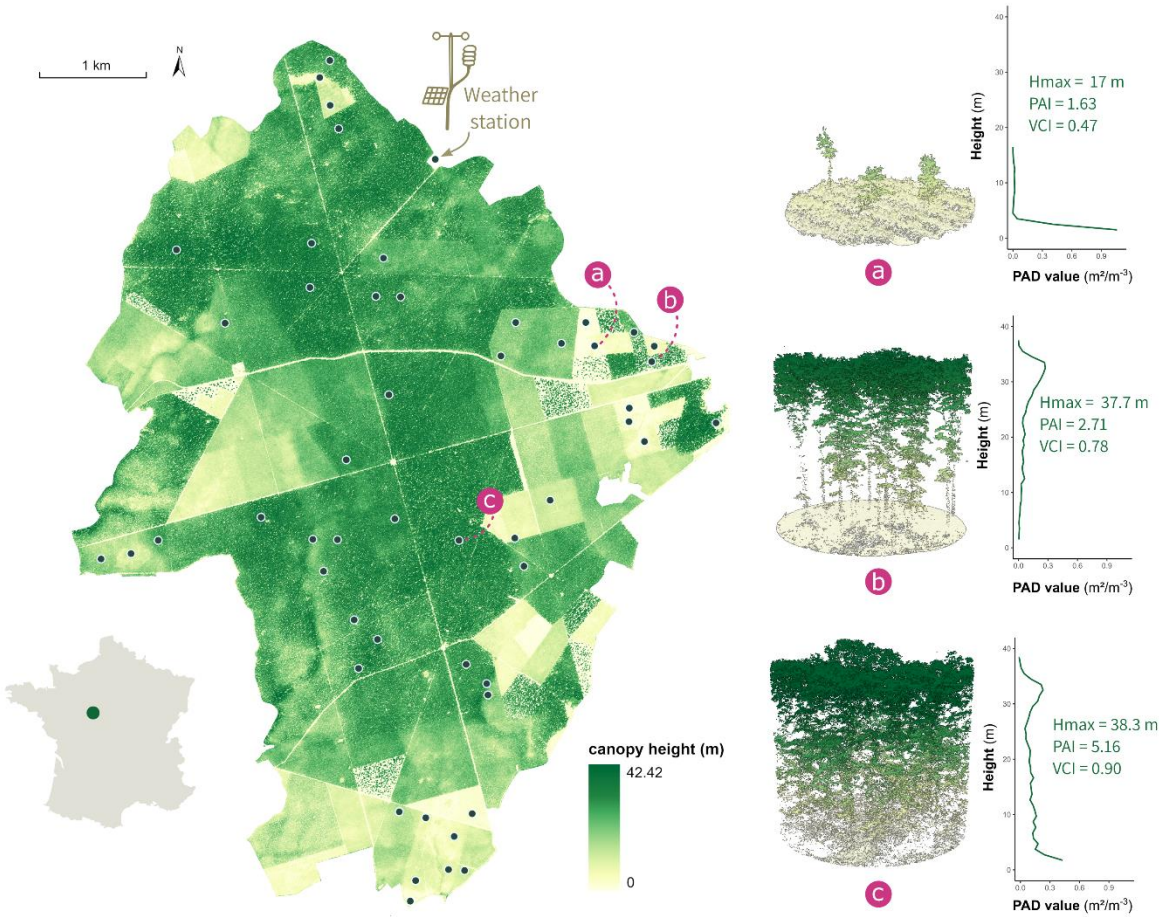

Fig. 2. Canopy height (at 50-cm resolution) over our study area, the forest of Blois (France). The dots depict the location of our study plots, with temperature sensors measuring air temperature. We show three contrasting examples of LiDAR point clouds, with their

associated plant area density (PAD) profile for a 20-m radius around the central plot. The colour scale on LiDAR profiles corresponds to canopy height as well.

2.4. Modelling the buffering or amplification impact of forest on microclimate

Using linear models, we related the log of the slope (extracted for each of our 53 focal sensors) to our three LiDAR-derived metrics. We compared the explanatory power of the three LiDAR-derived metrics, separately and jointly in each buffer size, by looking at the model r squared (R^2) (Kašpar et al., 2021).

For the multiple regression models, we checked for multicollinearity issues among our three predictors using the Variance Inflation Factor (VIF), which remained below the advisable threshold of 5 (Sheather, 2009) for each of the three variables. Hence, we kept all three LiDAR-derived variables as predictors in our multiple regression models, since the estimated coefficient values are still interpretable and trustworthy. Then, we calculated an independent R^2, root-mean-square error (RMSE) and mean absolute error (MAE) of the best model using a leave-one-out cross-validation, by rerunning the model iteratively with only 52 plots for calibration and the remaining plot for validation. Finally, we checked for a potential spatial autocorrelation signal in the residuals of the best model.

To print model coefficients, we used *tab_model* from the {sjPlot} package (Lüdecke, 2021), and to plot model predictions, *ggpredict* from the {ggeffects} package (Lüdecke, 2018). We used the {caret} package for the leave-one-out procedure (Kuhn, 2008). The correlogram of model residuals was built with the {ncf} package (Bjornstad and Cai, 2022).

2.5. Spatial predictions

2.5.1. Mapping the temperature buffering or amplification effect

To predict forest microclimate, we first calculated the three LiDAR-derived metrics over the whole forest of Blois, setting the spatial resolution of each raster map to the size of the buffer for which our model performed the best. Then, we used the estimated coefficients of our linear model to predict microclimate buffering or amplification (the log of the slope) in each pixel of the forest. Additionally, we mapped the standard error of predicted means over the entire forest in order to spot areas of higher uncertainty of our model, using the *predict* function as well. The microclimate of individual pixels was considered coupled to macroclimate temperature if the log of the slope was equal to 0 +/- the maximum error of the model, buffered if lower and amplified if higher. We used the R package {terra} and its dependencies to handle and represent spatial data (Hijmans et al., 2023).

2.5.2. Predicting and mapping point-in-time or mean microclimate temperature

Since the equilibrium parameter can be considered stable in a given macroclimate and season, we used the median of all 53 calculated equilibria over the leaf-on season (17.47°C) as the single equilibrium value for all predictions (Fig. S1, S2). For a given moment in time, the slope parameter (back-transformed, i.e. exp(log(slope))) is thus the only input variable that varies in space in the following equation: T_{micro} = slope x T_{macro} + equilibrium x (1 – slope). From the magnitude of this buffering or amplification effect, we predicted all hourly

microclimate temperature over the whole period on each of our 53 plots, from hourly macroclimate temperature recorded by the weather station. We tested the quality of these predictions of understory air temperature against the actual and matching hourly measurements made by the 53 sensors, by plotting predicted versus observed hourly temperatures. We computed the R^2, RMSE and MAE value of this observed versus predicted relationship.

Once the slope values are mapped over the entire forest, we can derive a map of subcanopy air temperature at any time (e.g. a given hour of a given day) if we know the corresponding macroclimate air temperature for that same time period (George et al., 2015). For illustrative purposes, we focused on the warmest day (14 August 2021) at the hour of maximum (15:00) and minimum (05:00) temperature that were recorded by the neighbouring weather station. We also mapped the mean of two daily statistics (daily minimum and maximum temperatures) over the whole June-September period. We assumed that no significant change in forest structure occurred during the period, as no extreme event such as fire or major timber harvesting was recorded. Daily minimum and maximum temperatures were extracted from the nearby weather station, used as the macroclimate temperature in our linear models (see equation above), and the mean statistics were plotted. We also calculated the resulting daily offsets to macroclimate (T_{micro} - T_{macro}).

Finally, we tested the assumption that the equilibrium can be considered constant over the whole study area by generating random equilibrium values following a normal distribution for each plot, using the mean and standard deviation of the observed equilibria. Using these random equilibrium values resulted in very similar, although slightly less well fitted temperature predictions (Appendix 4). We hence determined that using a constant

equilibrium fixed at the median introduced minimal error to temperature predictions, while vastly enhancing the ease and repeatability of this methodology.

3. Results

3.1 Computing slope and equilibrium from hourly temperatures

Temperatures recorded from June to September 2021 by the nearby weather station ranged from 4.1°C to 31.8°C, while it ranged from -1.1°C to 40.8°C across our 53 microclimatic sensors. The total range of air temperatures recorded simultaneously across our 53 sensors (i.e. difference between warmest and coolest temperature recorded by any sensor at a given time) averaged 5.5°C, with a maximum range of 18.2°C.

The sensor-specific linear regressions between macroclimate temperature and microclimate temperature to extract the slope and equilibrium parameters had very good fits (median R^2 = 93 %, ranging from 80.3 to 96 %; Fig. S1). We also compared these R^2 from linear regressions and the equivalent metric (the proportion of deviance explained) from non-linear GAMs. The fits were slightly better for GAMs, but overall very similar (mean difference = 0.2 %, maximum difference = 1 %), validating the linearity of the relationship between macroclimate and microclimate (Appendix 2).

The equilibrium was not exactly constant, ranging from 8.7 to 22.2°C around its median at 17.5°C (except for one outlier at - 102.5°C, resulting from a plot with a temperature highly coupled to macroclimate, i.e. a slope very close to 1, here 0.993). However, the equilibrium had a narrow quasi-normal distribution, with a standard deviation of 2.4°C around the mean

of 17.7°C without the outlier mentioned above (Fig. S1). As expected, the mean and median values of the equilibrium were close to the mean macroclimate value over the period (18.19°C). The log of the slope — of the regression between microclimate and macroclimate — ranged from -0.38 to +0.36 (Fig. S1).

3.2. Identifying the optimal resolution to explain microclimate buffering or amplification

Forest stand structure explained a large proportion of the observed variation in the log of the slope parameter, but with great disparities depending on the LiDAR-derived metric used as a predictor and the spatial resolution chosen to derive it (Fig. 3). The variable log(Hmax) had a very high predictive power (R^2 of 76 % to 80 %) from 1 m to 10 m-radius around the sensor location. The variables PAI and VCI both had lower explanatory power below a 5 m radius. Remarkably, while the explanatory power of log(Hmax) and VCI dropped after a 10 m-radius, PAI maintained roughly the same predictive power from 5 m to 70 m radius, even peaking at 20 m radius (Fig. 3). When the three predictors were used simultaneously in a single model, the model explaining most of the observed variation in the log of the slope was the one with LiDAR-derived predictors calculated for a 5 m radius (Table S1; R^2 = 91 %), albeit we note that from 3 m to 10 m, the R^2 remained very similar.

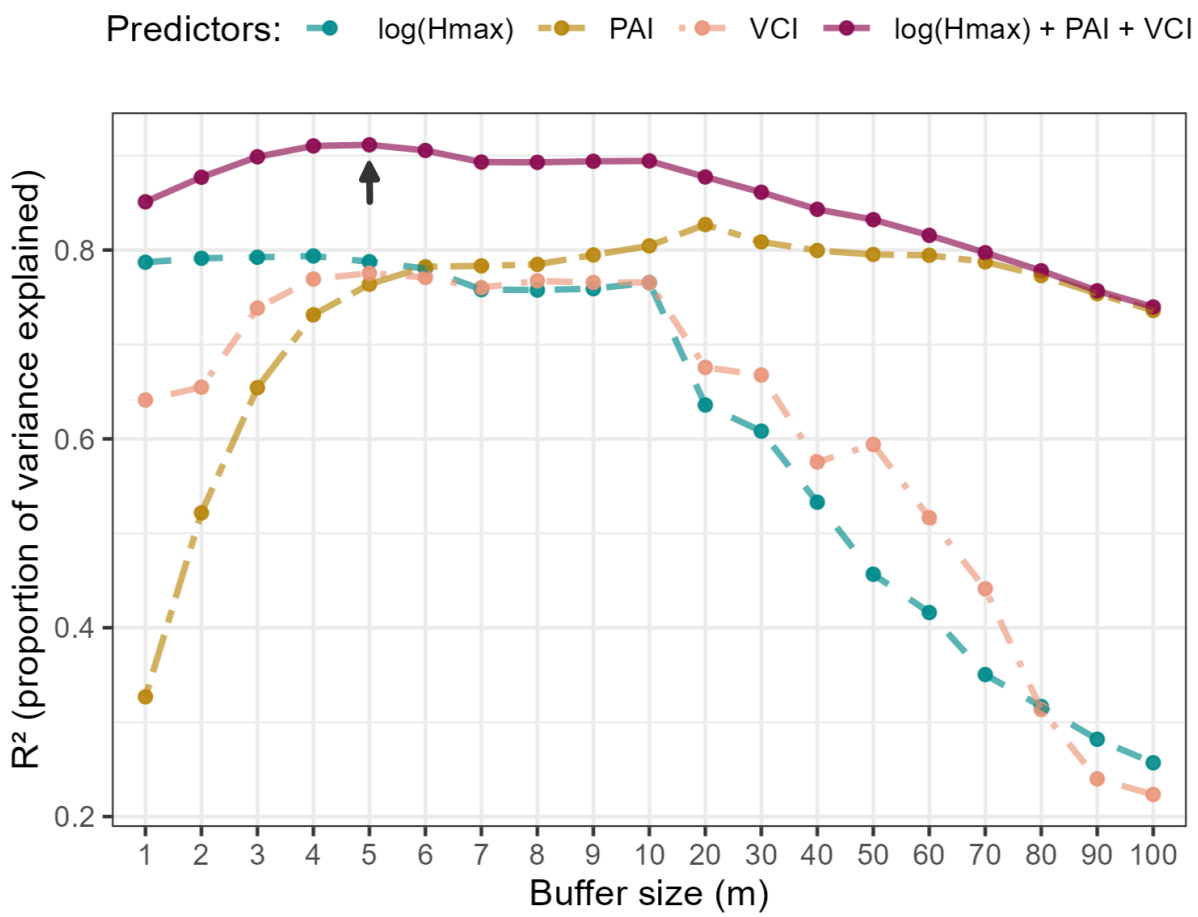

Fig. 3. Proportion of the observed variation in the log of the slope parameter (extracted from the linear relationship between microclimate and macroclimate temperatures) explained by each of the three LiDAR-derived predictors, separately (i.e. using simple linear regressions) and jointly (i.e. using a multiple linear regression). The proportion of explained variance was computed separately for each buffer radius: every metre from 1 to 10 m and then every 10 m from 10 to 100 m. The best radius (5 m, R^2 = 91 %) is highlighted with an arrow.

Irrespective of the spatial resolution (radius size) used, the three metrics had a negative effect on the log of the slope; taller trees and stands with high PAI and VCI values were more

buffered. The PAI and VCI variables had linear effects, while the maximum height had a non-linear effect after back transformation (Fig. 4).

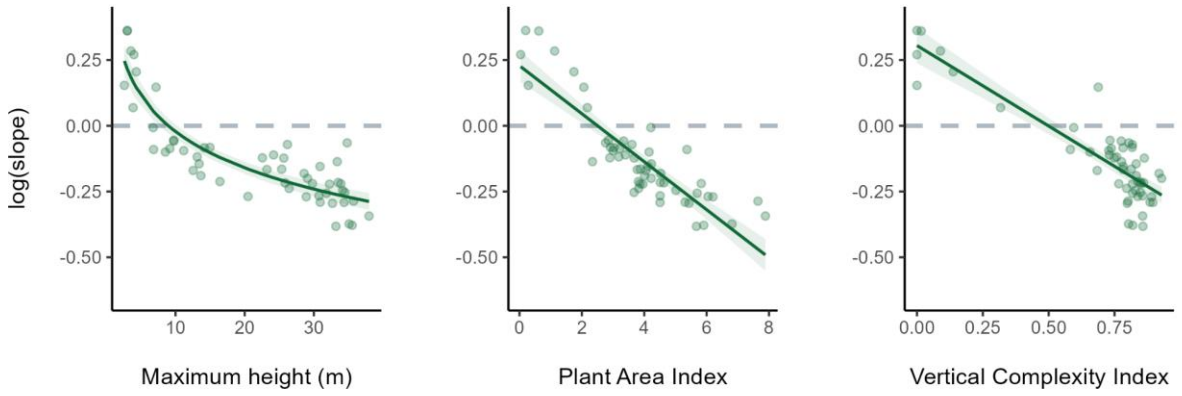

Fig. 4. Effect of LiDAR-derived variables related to stand structure on the log of the slope between microclimate and macroclimate temperatures. All LiDAR-derived variables depicted in this figure were computed for a 5 m radius buffer. Only univariate model predictions are illustrated here (see Fig. S5 for the predictions of the multivariate model). The log-transformation of the maximum height allowed us to linearize the relationship, and to use a simple linear model to predict microclimate effect. Here, the prediction is depicted with a back transformation – exp(log(Hmax)) – to show directly the effect of maximum height on the log of the slope parameter.

The R^2 of the model was 89 %, the RMSE was 0.059 and the MAE was 0.046 after a leave-one-out cross validation procedure (Fig. 5). Residuals of the models showed no spatial autocorrelation (Fig. S7).

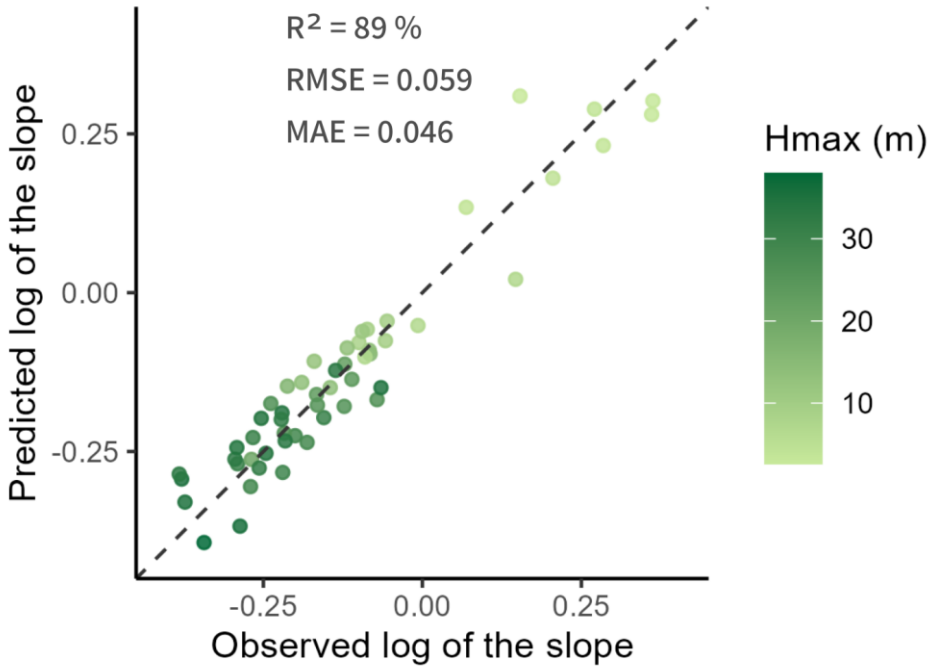

Fig. 5. Observed versus predicted log of the slope, from the best model with all three LiDAR-derived metrics at a 5-m buffer size, after a leave-one-out cross validation procedure. The colour gradient corresponds to the maximum height calculated around each plot with a 5-m buffer.

3.2. Mapping the buffering or amplification effect

Although the vast majority of the forest understory (91.4 % of the 275,500 10-m pixels covering the forest) had a buffered temperature compared to the standardised weather station (green colours on Fig. 6a), significant parts (5.9 %) of the forest had a coupled temperature that did not deviate significantly from the macroclimate (beige colours in Fig. 6a). Areas with low or sparse canopies (2.7 %) even showed the reverse trend, an

amplification of temperature with more extreme temperatures than recorded by the weather station (yellow colour in Fig. 6a).

Some areas showed more uncertainty in temperature predictions (darker red colours in Fig. 6b), typically in situations where the model had to extrapolate beyond the conditions observed in the calibration range. We indeed have a larger range of predicted log of the slope (- 0.59 to + 0.56) compared to the range of observed log of the slope (- 0.38 to + 0.36). This extrapolation concerned either stands with taller trees or denser and more complex vegetation layering or, alternatively, areas with very low, sparse and single layering of vegetation cover, such as road verges. The median standard error across the whole forest was 0.012, and the maximum 0.069 (Fig. 6, S6).

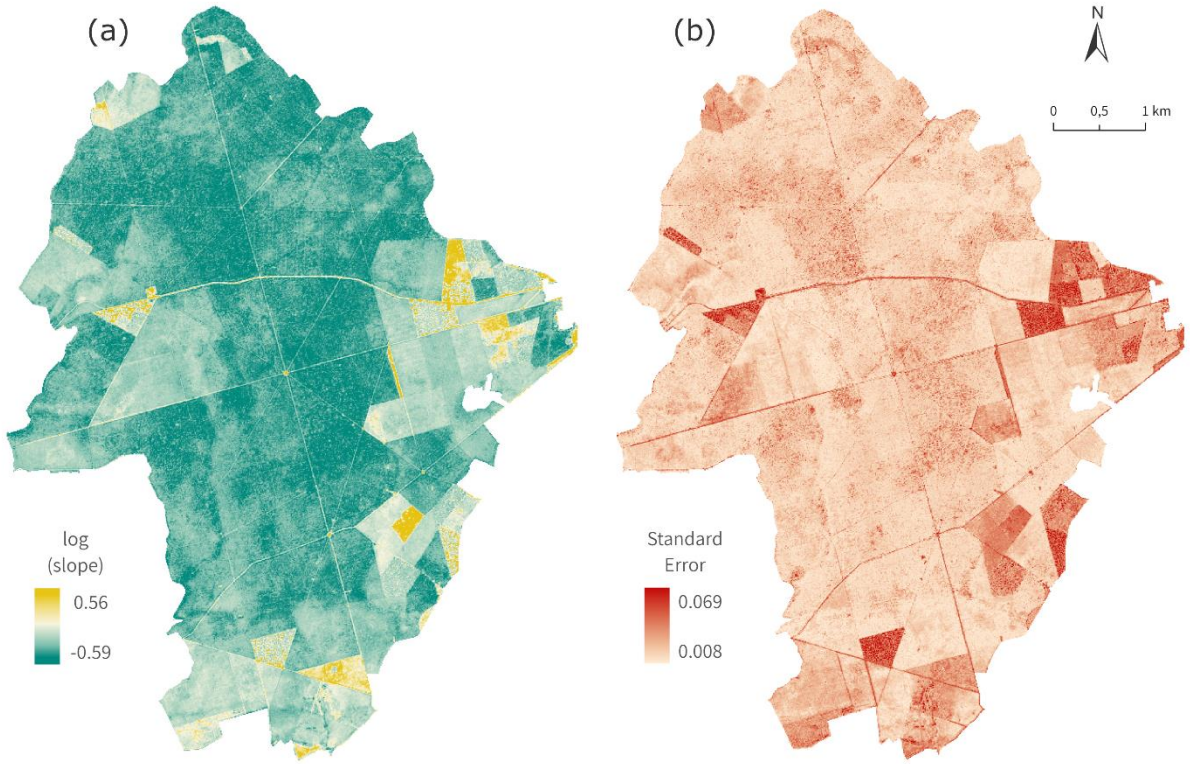

Fig. 6. Map of understory air temperature buffering or amplification over the forest of Blois (a), green for buffering, yellow for amplification, along with a map of the uncertainty of the predictions (b) by mapping the standard error – darker red colours suggest a higher uncertainty in predictions.

3.3. Predicting understory temperatures

Predicted understory temperatures (calculated from the predicted slope and median equilibrium) were indeed related to the matching observed temperatures of our 53 plots (R^2 = 91 %, Fig. 7). The RMSE was 1.2°C, and MAE was 0.9°C. Plots with amplified temperature had the greatest errors (Fig. 7, S10). If we separate plots were microclimate temperature is buffered (N = 45) from those where it is amplified (N = 7), model performance metrics showed an error in predicted hourly temperatures almost twice as large for amplified plot (R^2 = 87.9 %, RMSE = 1.95°C, MAE = 1.44°C, Fig. S10) compared to buffered plots (R^2 = 92.3 %, RMSE = 1.06°C, MAE = 0.79°C).

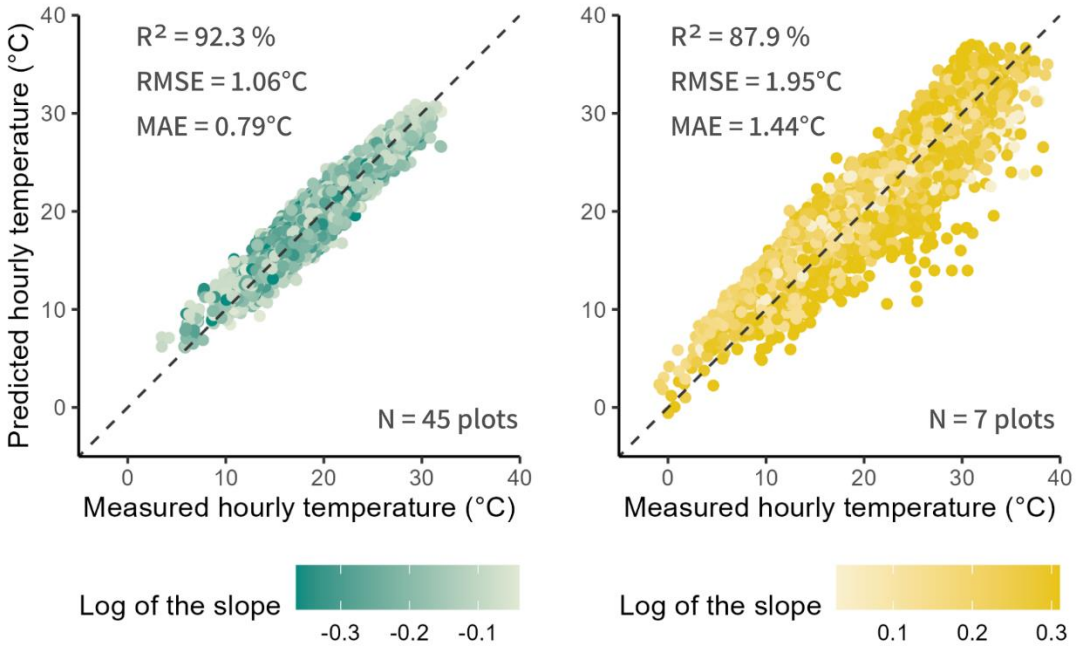

Fig. 7. Predicted versus observed hourly temperatures (random subset of n = 10,000 for each), separately for plots with a buffered temperature (log of the slope < 0, N = 45 plots, left) and with an amplified temperature (log of the slope > 0, N = 7 plots, right). Note that no plots have an exactly coupled temperature (log of the slope = 0). The colour gradient is the same as Fig. 6: green for buffered, and yellow for amplified plots. The model R^2, RMSE and MAE were calculated separately. For a similar figure with all plots at once, see Fig. S10.

Finally, as an illustration, we predicted the temperature on the 14th of August across the entire forest, focusing on the coolest (T_{macro} = 14.3°C) and warmest (T_{macro} = 31.8°C) hours of that day (5:00 and 15:00, respectively), according to the nearby weather station. At 05:00, the total range of predicted microclimate temperature was 3.8°C – from 11.9 to 15.7°C). At 15:00, the range was 17.2°C – from 25.4 to 42.6°C (Fig. 8). We also predicted the mean of daily statistics over the studied period across the forest: mean minimum temperature

ranged from 8.4 to 14.6°C and mean maximum temperature from 21.4 to 29.9°C (Fig. S8). Daily offsets (microclimate minus macroclimate) of maximum temperatures from all days from June to September ranged from - 5°C to + 13.2°C, and for minimum temperature from - 6.4°C to + 4.5°C (Fig. S9).

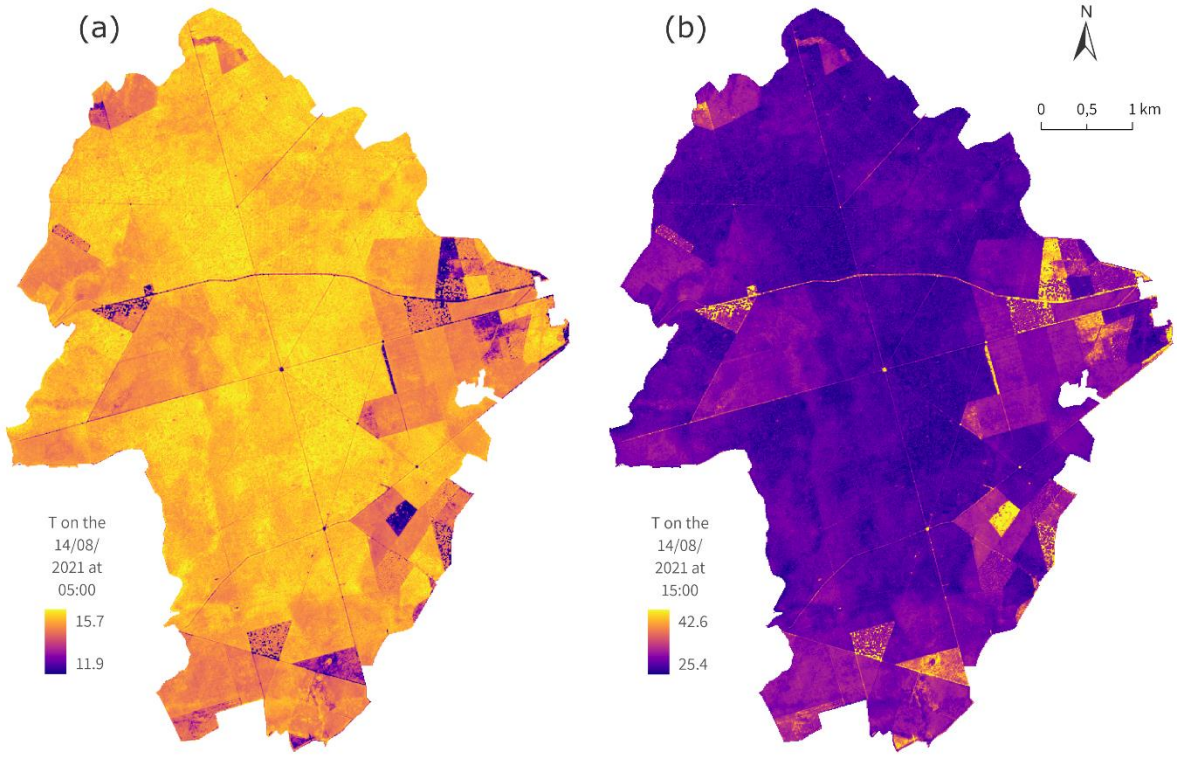

Fig. 8. Predicted air temperature at 1-metre high for (a) the warmest (T_{macro} = 31.8°C) and (b) the coldest (T_{macro} = 14.3°C) time of the warmest day, according to the nearby weather station, during summer 2021 (14th of August, 15:00 and 05:00 respectively) in the forest of Blois. The spatial resolution of the predictions is 10 m. Note that the colour scale corresponds to different ranges of temperature in (a) and (b). See Fig. S8 for similar maps,

but instead of point-in-time temperature, two statistics of understory air temperature: the mean of daily maxima and the mean of daily minima during summer 2021.

4. Discussion

4.1. Using LiDAR to relate forest structure to temperature buffering or amplification

We showed that three metrics derived from airborne LiDAR that describe forest structure – maximum canopy height, plant area index (PAI), and vertical complexity index (VCI) – can be sufficient to map understory air temperature. Errors increased under very open vegetation cover, similarly to former findings from George et al. (2015), with errors in predicted temperatures doubling (from 1 to 2°C) in amplified habitats compared to buffered ones. However, our rather simple linear model with LiDAR predictors had a very good explanatory power on microclimate (R^2 = 91 %), resulting in good performance as well in hourly temperature predictions, validated against observations (R^2 = 91 % over all plots, 89 % in amplified plots, 92 % in buffered plots).

The effects of our three predictors are consistent with what has been reported so far in the scientific literature. First, maximum height is known to drive microclimate temperature (Frey et al., 2016; George et al., 2015; Kašpar et al., 2021). Here, using the log transformation, we confirm a non-linear effect of vegetation height on the magnitude of the buffering effect: an increase in the first metres of height has a greater impact on microclimate, similarly to former work by Jucker et al. (2018). Second, leaf or plant area index (LAI or PAI) are among

the best predictors of microclimate temperature beneath trees canopies (Hardwick et al., 2015; Jucker et al., 2018). Note that whenever the term LAI is employed, it often actually is PAI, since discriminating leaves from trunks and branches from airborne LiDAR point clouds or other methods remains challenging. One of the main advantages of PAI is that it integrates not only the top canopy, but also the vegetation layering underneath (Lenoir et al., 2022), information that is lacking when considering canopy structure from 2D optical imagery or photogrammetric products (Marsh et al., 2022). The sub-canopy and understory layers are indeed significant drivers of microclimate (Kovács et al., 2017; Stickley and Fraterrigo, 2021). Third, VCI complements this information, also accounting for vegetation layering underneath the upper canopy, but rather focusing on the evenness of its vertical distribution. Even though VCI was used to describe forest succession (van Ewijk et al., 2011), to our knowledge, it has not yet been used as a microclimate predictor. We argue for its use as a major metric quantifying the vertical complexity in future endeavours to model microclimate.

A taller forest stand with massive aboveground and well-distributed foliage can be compared to a thicker, denser, and multi-layered insulating material, resulting in an enhanced buffering capacity (De Frenne et al., 2021; Frey et al., 2016; Jucker et al., 2018). On the other hand, our study shows that a forest with a low canopy and reduced PAI and VCI has the opposite effect on temperature. Microclimate amplification is a known phenomenon (Woods et al., 2021), but it is much less often considered than buffering, for which we hypothesise two main reasons. First, open areas are often discarded because low cost microclimate sensors, even if shielded, are less reliable in exposed conditions and prone to overheating (Maclean et al., 2021; Terando et al., 2017). Nevertheless, organisms are also subjected to overheating if they stand in full sun, and microclimate temperature sensors placed directly near the habitat

of interest could be more ecologically relevant than standardised, unbiased weather stations (Ashcroft, 2018). The warmer or cooler temperatures we recorded in open areas are thus likely to be relevant from a living organism perspective, even if prone to higher measurement uncertainties – and even if living organism are likely to have different thermal properties than temperature sensors. Second, open areas are often used as references, proxies for macroclimate, and are not the focus of most forest microclimate studies. However, open or sparsely vegetated areas are very common either in managed (regeneration stages, roads, intraforest clearings) or natural (canopy gaps, savannah, rock boulders) forested landscapes (Kovács et al., 2017; Pincebourde and Suppo, 2016; Tymen et al., 2017) and deserve to be studied as components of forest environments. Moreover, close to edges or under a certain threshold of PAI, even forested areas can show patterns of temperature amplification (von Arx et al., 2013; Williamson et al., 2021). Beyond forests, open habitats such as crops, peatlands or deserts have a temperature that may deviate substantially from weather station temperature and exhibit strong spatial heterogeneity in microclimates as well. We therefore recommend a generalised approach, integrating both buffered and amplified microclimates in future investigations.

4.2. Choosing the best scale to assess forest structure and microclimate

Our three LiDAR-derived variables that describe forest structure all had a very high explanatory power on the slope parameter when they were calculated in radii from 5 to 10 m (R^2 > 76 %), which is smaller than the representative spatial grain for similar forest

structure metrics (25 to 75 m resolution) determined by Atkins et al. (2023). Beyond a 10 m radius, the predictive power of log(Hmax) and VCI abruptly dropped, while PAI remained highly informative up to a 70 m radius. Contrary to PAI and VCI, log(Hmax) was a good predictor at very fine spatial resolutions, even as low as a 1 m radius. Smith-Tripp et al. (2022) used photogrammetry to calculate canopy height, and found that the best explaining scale on microclimate temperature was 15 m, a slightly larger scale than the one we identified, but still close to our results. Kašpar et al. (2021) and Frey et al. (2016) found coarser resolutions as the most informative, but the latter only tested a resolution of 25 and 250 metres. The optimal resolution may vary according to the stand type, and be point-density or -intensity dependent, in relation with the height of flight and LiDAR sensor properties like pulse frequency. For instance, in dense tropical rainforests, comparable results could be obtained only with very high-density LiDAR data. Therefore, results may not be strictly comparable across studies. As such, the scale of effect of metrics should always be tested when considering new airborne LiDAR datasets (Atkins et al., 2023).

Another potential issue is the accuracy of their Global Navigation Satellite System (GNSS), which can be much lower than specified by manufacturers under forest cover (Naesset and Jonmeister, 2002). When choosing very small spatial resolutions (1 to 3 m buffer) for LiDAR-derived metrics, the microclimate temperature sensor may in fact, due to the poor accuracy of GPS coordinates in forests, be located outside the area under consideration (Atkins et al., 2023). We advise not to choose a scale that is too small, if the accuracy of sensor localisation from GPS cannot match it. Instead, to further improve the resolution of microclimate temperature maps, another solution could be to keep a 5 to 10-m sized buffer, but derive metrics in “moving windows”, a technique often used to “soften” images and to derive

textural information in landscape ecology (Hagen-Zanker, 2016). There are few applications with LiDAR data, as processing time can be very long considering the huge datasets.

Whether we should always strive to the greatest possible accuracy depends on the scientific question, the organisms under study or ecological patterns we want to explain, and the application envisioned (Bennie et al., 2014). We do need ecologically-relevant maps, with spatial resolutions meaningful for biodiversity or management (Bramer et al., 2018; Zellweger et al., 2019b). For instance, a common resolution used for floristic inventories in forests is 400 m² (corresponding to an 11.3-m radius). Making maps with a 2 m resolution will not necessarily be useful to explain processes happening within the proximal resolution of understory plant communities, although information on within-plot microclimate diversity could be useful to explore plant distribution. In other situations, sub-meter resolution may be relevant, for instance, if one wants to study whether tree holes or epiphytes can efficiently protect tropical frogs against lethal temperatures (Scheffers et al., 2014). If so, terrestrial or UAV-borne sensors can help to take an even closer look at forest structure, spot such microhabitats and predict their buffering capacity (Hoffrén and García, 2023).

4.3. Beyond LiDAR-based vegetation structure

Forest structure is hardly the only driver of microclimate temperature buffering: topography or hydrology can play major roles as well (Greiser et al., 2018; Jucker et al., 2018; Zellweger et al., 2019a). For instance, northern-oriented slopes or places characterised by higher soil moisture are associated with a higher microclimate temperature buffering potential (Hoffrén and García, 2023; Zellweger et al., 2019a). The distance to water bodies or rivers is another

major driver described in the scientific literature (McLaughlin et al., 2017). In our case, the Topographic Wetness Index and distance to the nearest river were calculated and had no significant effect (see Fig. S3, S4), probably because the area is fairly flat, and the forest of Blois does not have any large, permanent rivers in its boundaries. However, depending on the context, these variables should be included in predictive models as well.

Another category of relevant metrics involves landscape features, such as the proportion of forest cover in a wide buffer or the distance to the nearest forest edge (Meeussen et al., 2021). However, our sampling design did not allow us to test for these landscape effects on the magnitude of the buffering or amplification effect. Adding the effect of edges to our models would have necessitated a different protocol, with several sensors placed along a gradient of edge distances, including intraforest edges such as clearings or roads that cross the forest of Blois. Future endeavours to spatialise microclimate temperature or other variables such as relative humidity could focus on this question of forest edges to improve resulting maps.

Lastly, especially so in a managed forest, the buffering or amplification capacity will be dynamic over time, as thinning or harvest practices will drastically impact the resulting microclimate effect and its spatial distribution. Up-to-date data is required to reflect the result of forestry management (Greiser et al., 2018). Unfortunately, the high costs of an airborne LiDAR campaign make it hard to repeat acquisitions in time. However, other remote sensing techniques such as photogrammetry may help to fill this gap and obtain a temporal series of forest structure from optical images (Randin et al., 2020). Spaceborne radar data, for example Sentinel-1 time-series, has the potential to provide variables sensitive to

changes in forest structure that have proven their utility in biodiversity modelling (Bae et al., 2019).

Coupled with Sentinel-2 multispectral imagery, radar could deliver relevant predictors at high spatial resolution (10 m) and high temporal resolution (two or more images per month). Combining LiDAR with other remote sensing techniques may also be useful to obtain information complementary to structure, such as canopy phenology or water status (Zellweger et al., 2019b).

4.4. Applications: why map forest temperature buffering or amplification?

We propose to model one integrative and mechanistic metric representing the microclimate effect (the "log of the slope"). This approach differs from modelling offsets (the difference between macroclimate and microclimate) or temperature itself (Gril et al., 2023). For instance, Davis et al. (2019), Frey et al. (2016) and George et al. (2015) modelled directly daily or sub-daily temperatures, or statistics such as the mean minimum and maximum temperature as response variables. With our parsimonious approach, once the buffering or amplification capacity is modelled, we simply need the equilibrium to infer the whole linear relationship between microclimate and macroclimate. Although it is likely to contribute to predictions errors, the equilibrium can be considered constant in a given site (e.g. one forest) and fixed at its median, or approached by mean macroclimate. Then we have enough information to easily retrieve any point-in-time or statistic of microclimate temperature. The only thing needed is macroclimate temperature data with a matching temporal resolution,

either using nearby weather stations or global databases such as ERA5 or E-OBS, with hourly macroclimate temperature at coarse spatial resolutions (Cornes et al., 2018; Muñoz-Sabater et al., 2021). Spatializing this forest buffering or amplification effect can have multiple applications (Zellweger et al., 2019b). Here, we listed a few examples of how such a map can be useful, aside from inferring any microclimate temperature of the understory.

(1) To study one of the many temperature-related processes, such as thermoregulation (Milling et al., 2018), photosynthesis (Miller et al., 2021) or phenology (Jackson, 1966), as forest understory species may not only have adapted to temperature itself, but also to temperature range and variation through time.

(2) To model the thermal connectivity of habitats at the landscape level, and build current density maps based on a fine-scale spatialized buffering effect (Huang et al., 2022; Milanesi et al., 2017). Some forest-dwelling species (such as insects, birds, amphibians or ungulates) have to move daily or seasonally for foraging, mating or nesting. Here, road verges or clear-cut areas with amplified temperatures may impair the thermal connectivity for forest specialists (e.g. the buffered forest stands located east of the forest of Blois may be hard to reach for some species, as they are surrounded by areas with large temperature amplification).

(3) To improve species distribution and redistribution models with climate change, and to spot thermal microrefugia with buffered climatic conditions (Lenoir et al., 2017). Species distribution models incorporating microclimate may yield great discrepancies compared to the usual ones based on macroclimatic grids (Haesen et al. 2023; Stickley and Fraterrigo, 2023). Local extinction risks and thermophilization, i.e. the gain of warm-adapted and loss of cold-adapted taxa, may be mitigated by the thermal insulating function of forest canopies

(Zellweger et al., 2020). This is especially relevant to the conservation of threatened understory species facing climate change, and to prioritise suitable refuges that may represent long-term microrefugia. Adding directly a metric quantifying the buffering or amplification effect as a predictor of species distributions might be a great step forward.

(4) To assist forest management decisions under climate change. For foresters, this kind of map may help, for instance, to evaluate the risk for tree regeneration, as young seedlings and saplings are especially sensitive to climatic extremes (von Arx et al., 2013). Sessile oaks seedlings have been shown to be sensitive to local microclimatic gradients, in terms of germination, survival and performance (Meeussen et al., 2022). We found that all regeneration stages in our study forest, with low or sparse canopy, were subjected to strong amplification of temperature extremes. This means more exposure to frost or heat shock, in addition to the risks of drought associated with high temperatures. Forestry has a central role in mitigating local effects of global warming through microclimate regulation (Christiansen et al., 2022; Greiser et al., 2018). Another “burning issue” in forest management is wildfire control, and these areas of amplified temperature extremes should be especially at risk, deserving close surveillance (Laurance, 2004).

(5) To make informed decisions about landscape planning for a human-liveable future, especially in the case of urban forests such as the forest of Blois. Predictive models may supply managers with site-specific, quantitative advice on how to strengthen urban forest buffering capacity by manipulating forest structures. A map of forest microclimate effect may also help to select cool spots that may act as cooling recreational areas to humans during heatwaves, and create safe havens and walkable paths to escape the dreaded urban heat island effect (Gillerot et al., 2022).

In brief, this study brings interesting prospects towards efficiently obtaining maps of forest structure and microclimates, as airborne LiDAR point clouds are becoming more and more available in Europe and beyond (Moudrý et al., 2022). We hope our flexible approach will be applied across different biomes and forest types, with LiDAR or other remote sensing technologies, for high-resolution maps of forest thermal environments.

Acknowledgements

We deeply thank all interns who contributed to temperature data collection in the field, namely Hugo Mahier, Germain Vital, Ambre Châline, and Hugo Hayé. We also thank the French National Forest Office (ONF) and all ONF agents who helped with the project.

We thank Jérôme Chaves, Rebecca Senior and one anonymous reviewer, for their insightful comments and suggestions which strengthened and clarified our paper.

J.L. acknowledges funding from the Centre National de la Recherche Scientifique (CNRS), under the framework of the Mission pour les Initiatives Transverses et Interdisciplinaires (MITI, Défi INFINITI 2018: MORFO project), and the Agence Nationale de la Recherche (ANR), under the framework of the young investigators' funding scheme (JCJC Grant N°ANR-19-CE32-0005-01: IMPRINT project) which funded E.G.'s PhD. S.H. received funding from a FLOF fellowship of the KU Leuven (project nr. 3E190655).

Conflict of Interest

None.

Author's contributions

JL, EGM, FS and RM designed and performed the experiment, and collected field data along with BB, EG and VLR. EGM, ML and SD handled the collection and treatment of LiDAR data. EG performed the analysis with ML, JL and RM. GD, JL, KVM, RM, SD and SH participated in the writing lead by EG.

All authors significantly contributed to this study and agreed to the submission of this draft.

Data and Code Availability

The R Markdown script and data are available online on Figshare (private link for the review process: https://figshare.com/s/6f9beb675f3ea927b48d).

References

Ashcroft, M.B., 2018. Which is more biased: Standardized weather stations or microclimatic sensors? Ecology and Evolution 8, 5231–5232. https://doi.org/10.1002/ece3.3965

Atkins, J.W., Costanza, J., Dahlin, K.M., Dannenberg, M.P., Elmore, A.J., Fitzpatrick, M.C., Hakkenberg, C.R., Hardiman, B.S., Kamoske, A., LaRue, E.A., Silva, C.A., Stovall, A.E.L.,

Tielens, E.K., 2023. Scale dependency of lidar-derived forest structural diversity. Methods in Ecology and Evolution 14, 708–723. https://doi.org/10.1111/2041-210X.14040

Bae, S., Levick, S.R., Heidrich, L., Magdon, P., Leutner, B.F., Wöllauer, S., Serebryanyk, A., Nauss, T., Krzystek, P., Gossner, M.M., Schall, P., Heibl, C., Bässler, C., Doerfler, I., Schulze, E.-D., Krah, F.-S., Culmsee, H., Jung, K., Heurich, M., Fischer, M., Seibold, S., Thorn, S., Gerlach, T., Hothorn, T., Weisser, W.W., Müller, J., 2019. Radar vision in the mapping of forest biodiversity from space. Nat Commun 10, 4757. https://doi.org/10.1038/s41467-019-12737-x

Bennie, J., Wilson, R.J., Maclean, I.M.D., Suggitt, A.J., 2014. Seeing the woods for the trees – when is microclimate important in species distribution models? Global Change Biology 20, 2699–2700. https://doi.org/10.1111/gcb.12525

Bjornstad, O.N., Cai, J., 2022. ncf: Spatial Covariance Functions.

Bramer, I., Anderson, B.J., Bennie, J., Bladon, A.J., De Frenne, P., Hemming, D., Hill, R.A., Kearney, M.R., Körner, C., Korstjens, A.H., Lenoir, J., Maclean, I.M.D., Marsh, C.D., Morecroft, M.D., Ohlemüller, R., Slater, H.D., Suggitt, A.J., Zellweger, F., Gillingham, P.K., 2018. Advances in Monitoring and Modelling Climate at Ecologically Relevant Scales, in: Bohan, D.A., Dumbrell, A.J., Woodward, G., Jackson, M. (Eds.), Advances in Ecological Research, Next Generation Biomonitoring: Part 1. Academic Press, pp. 101–161. https://doi.org/10.1016/bs.aecr.2017.12.005

Bouvier, M., Durrieu, S., Fournier, R.A., Renaud, J.-P., 2015. Generalizing predictive models of forest inventory attributes using an area-based approach with airborne LiDAR data. Remote Sensing of Environment 156, 322–334. https://doi.org/10.1016/j.rse.2014.10.004

Chen, J., Saunders, S.C., Crow, T.R., Naiman, R.J., Brosofske, K.D., Mroz, G.D., Brookshire, B.L., Franklin, J.F., 1999. Microclimate in Forest Ecosystem and Landscape Ecology: Variations in local climate can be used to monitor and compare the effects of different management regimes. BioScience 49, 288–297. https://doi.org/10.2307/1313612

Christiansen, D.M., Iversen, L.L., Ehrlén, J., Hylander, K., 2022. Changes in forest structure drive temperature preferences of boreal understorey plant communities. Journal of Ecology 110, 631–643. https://doi.org/10.1111/1365-2745.13825

Cornes, R.C., van der Schrier, G., van den Besselaar, E.J.M., Jones, P.D., 2018. An Ensemble Version of the E-OBS Temperature and Precipitation Data Sets. Journal of Geophysical Research: Atmospheres 123, 9391–9409. https://doi.org/10.1029/2017JD028200

Davis, F.W., Synes, N.W., Fricker, G.A., McCullough, I.M., Serra-Diaz, J.M., Franklin, J., Flint, A.L., 2019. LiDAR-derived topography and forest structure predict fine-scale variation in daily surface temperatures in oak savanna and conifer forest landscapes. Agricultural and Forest Meteorology 269–270, 192–202. https://doi.org/10.1016/j.agrformet.2019.02.015

De Frenne, P., Verheyen, K., 2016. Weather stations lack forest data. Science 351, 234–234. https://doi.org/10.1126/science.351.6270.234-a

De Frenne, P., Lenoir, J., Luoto, M., Scheffers, B.R., Zellweger, F., Aalto, J., Ashcroft, M.B., Christiansen, D.M., Decocq, G., Pauw, K.D., Govaert, S., Greiser, C., Gril, E., Hampe, A., Jucker, T., Klinges, D.H., Koelemeijer, I.A., Lembrechts, J.J., Marrec, R., Meeussen, C., Ogée, J., Tyystjärvi, V., Vangansbeke, P., Hylander, K., 2021. Forest microclimates and climate change: Importance, drivers and future research agenda. Global Change Biology 27, 2279–2297. https://doi.org/10.1111/gcb.15569

Frey, S.J.K., Hadley, A.S., Johnson, S.L., Schulze, M., Jones, J.A., Betts, M.G., 2016. Spatial models reveal the microclimatic buffering capacity of old-growth forests. Science Advances 2, e1501392. https://doi.org/10.1126/sciadv.1501392

Geiger, R., Aron, R.H., Todhunter, P., 2003. The Climate Near the Ground. Rowman & Littlefield.

George, A.D., Thompson, F.R., Faaborg, J., 2015. Using LiDAR and remote microclimate loggers to downscale near-surface air temperatures for site-level studies. Remote Sensing Letters 6, 924–932. https://doi.org/10.1080/2150704X.2015.1088671

Greiser, C., Meineri, E., Luoto, M., Ehrlén, J., Hylander, K., 2018. Monthly microclimate models in a managed boreal forest landscape. Agricultural and Forest Meteorology 250–251, 147–158. https://doi.org/10.1016/j.agrformet.2017.12.252

Gril, E., Spicher, F., Greiser, C., Ashcroft, M.B., Pincebourde, S., Durrieu, S., Nicolas, M., Richard, B., Decocq, G., Marrec, R., Lenoir, J., 2023. Slope and equilibrium: A parsimonious and flexible approach to model microclimate. Methods in Ecology and Evolution n/a. https://doi.org/10.1111/2041-210X.14048

Grolemund, G., Wickham, H., 2011. Dates and Times Made Easy with lubridate. Journal of Statistical Software 40, 1–25. https://doi.org/10.18637/jss.v040.i03

Gillerot, L., Landuyt, D., Oh, R., Chow, W., Haluza, D., Ponette, Q., Jactel, H., Bruelheide, H., Jaroszewicz, B., Scherer-Lorenzen, M., De Frenne, P., Muys, B., Verheyen, K., 2022. Forest structure and composition alleviate human thermal stress. Global Change Biology 28, 7340–7352. https://doi.org/10.1111/gcb.16419

Haesen, S., Lembrechts, J.J., De Frenne, P., Lenoir, J., Aalto, J., Ashcroft, M.B., Kopecký, M., Luoto, M., Maclean, I., Nijs, I., Niittynen, P., van den Hoogen, J., Arriga, N., Brůna, J., Buchmann, N., Čiliak, M., Collalti, A., De Lombaerde, E., Descombes, P., Gharun, M., Goded, I., Govaert, S., Greiser, C., Grelle, A., Gruening, C., Hederová, L., Hylander, K., Kreyling, J., Kruijt, B., Macek, M., Máliš, F., Man, M., Manca, G., Matula, R., Meeussen, C., Merinero, S., Minerbi, S., Montagnani, L., Muffler, L., Ogaya, R., Penuelas, J., Plichta, R., Portillo-Estrada, M., Schmeddes, J., Shekhar, A., Spicher, F., Ujházyová, M., Vangansbeke, P., Weigel, R., Wild, J., Zellweger, F., Van Meerbeek, K., 2021. ForestTemp – Sub-canopy microclimate temperatures of European forests. Global Change Biology 27, 6307–6319. https://doi.org/10.1111/gcb.15892

Haesen, S., Lenoir, J., Gril, E., De Frenne, P., Lembrechts, J., Kopecký, M., Macek, M., Man, M., Wild, J., Meerbeek, K.V., 2023. Uncovering the hidden niche: incorporating

microclimate temperature into species distribution models. https://doi.org/10.32942/X21600

Hagen-Zanker, A., 2016. A computational framework for generalized moving windows and its application to landscape pattern analysis. International Journal of Applied Earth Observation and Geoinformation 44, 205–216. https://doi.org/10.1016/j.jag.2015.09.010

Hardwick, S.R., Toumi, R., Pfeifer, M., Turner, E.C., Nilus, R., Ewers, R.M., 2015. The relationship between leaf area index and microclimate in tropical forest and oil palm plantation: Forest disturbance drives changes in microclimate. Agricultural and Forest Meteorology 201, 187–195. https://doi.org/10.1016/j.agrformet.2014.11.010

Hijmans, R.J., Bivand, R., Pebesma, E., Sumner, M.D., 2023. terra: Spatial Data Analysis.

Hoffrén, R., García, M.B., 2023. Thermal unmanned aerial vehicles for the identification of microclimatic refugia in topographically complex areas. Remote Sensing of Environment 286, 113427. https://doi.org/10.1016/j.rse.2022.113427

Huang, A., Shen, R., Jia, G., Xu, X., 2022. Reforestation enhanced landscape connectivity for thermal buffering in China. Environ. Res. Lett. 17, 014056. https://doi.org/10.1088/1748-9326/ac3fda

Jackson, M.T., 1966. Effects of Microclimate on Spring Flowering Phenology. Ecology 47, 407–415. https://doi.org/10.2307/1932980

Jucker, T., Hardwick, S.R., Both, S., Elias, D.M.O., Ewers, R.M., Milodowski, D.T., Swinfield, T., Coomes, D.A., 2018. Canopy structure and topography jointly constrain the microclimate of human-modified tropical landscapes. Global Change Biology 24, 5243–5258. https://doi.org/10.1111/gcb.14415

Joly, D., Brossard, T., Cardot, H., Cavailhes, J., Hilal, M., Wavresky, P., 2010. Les types de climats en France, une construction spatiale. Cybergeo : European Journal of Geography. https://doi.org/10.4000/cybergeo.23155

Kašpar, V., Hederová, L., Macek, M., Müllerová, J., Prošek, J., Surový, P., Wild, J., Kopecký, M., 2021. Temperature buffering in temperate forests: Comparing microclimate models based on ground measurements with active and passive remote sensing. Remote Sensing of Environment 263, 112522. https://doi.org/10.1016/j.rse.2021.112522

Kovács, B., Tinya, F., Ódor, P., 2017. Stand structural drivers of microclimate in mature temperate mixed forests. Agricultural and Forest Meteorology 234–235, 11–21. https://doi.org/10.1016/j.agrformet.2016.11.268

Kuhn, M., 2008. Building Predictive Models in R Using the caret Package. Journal of Statistical Software 28, 1–26. https://doi.org/10.18637/jss.v028.i05

Laurance, W.F., 2004. Forest-climate interactions in fragmented tropical landscapes. Philosophical Transactions of the Royal Society of London. Series B: Biological Sciences 359, 345–352. https://doi.org/10.1098/rstb.2003.1430

Lembrechts, J.J., Aalto, J., Ashcroft, M.B., De Frenne, P., Kopecký, M., Lenoir, J., Luoto, M., Maclean, I.M.D., Roupsard, O., Fuentes-Lillo, E., García, R.A., Pellissier, L., Pitteloud, C., Alatalo, J.M., Smith, S.W., Björk, R.G., Muffler, L., Backes, A.R., Cesarz, S., Gottschall, F., Okello, J., Urban, J., Plichta, R., Svátek, M., Phartyal, S.S., Wipf, S., Eisenhauer, N., Puşcaş, M., Turtureanu, P.D., Varlagin, A., Dimarco, R.D., Jump, A.S., Randall, K., Dorrepaal, E., Larson, K., Walz, J., Vitale, L., Svoboda, M., Higgens, R.F., Halbritter, A.H., Curasi, S.R., Klupar, I., Koontz, A., Pearse, W.D., Simpson, E., Stemkovski, M., Graae, B.J., Sørensen, M.V., Høye, T.T., Calzado, M.R.F., Lorite, J., Carbognani, M., Tomaselli, M., Forte, T.G.W., Petraglia, A., Haesen, S., Somers, B., Meerbeek, K.V., Björkman, M.P., Hylander, K., Merinero, S., Gharun, M., Buchmann, N., Dolezal, J., Matula, R., Thomas, A.D., Bailey, J.J., Ghosn, D., Kazakis, G., Pablo, M.A. de, Kemppinen, J., Niittynen, P., Rew, L., Seipel, T., Larson, C., Speed, J.D.M., Ardö, J., Cannone, N., Guglielmin, M., Malfasi, F., Bader, M.Y., Canessa, R., Stanisci, A., Kreyling, J., Schmeddes, J., Teuber, L., Aschero, V., Čiliak, M., Máliš, F., Smedt, P.D., Govaert, S., Meeussen, C., Vangansbeke, P., Gigauri, K., Lamprecht, A., Pauli, H., Steinbauer, K., Winkler, M., Ueyama, M., Nuñez, M.A., Ursu, T.-M., Haider, S., Wedegärtner, R.E.M., Smiljanic, M., Trouillier, M., Wilmking, M., Altman, J., Brůna, J., Hederová, L., Macek, M., Man, M., Wild, J., Vittoz, P., Pärtel, M., Barančok, P., Kanka, R., Kollár, J., Palaj, A., Barros, A., Mazzolari, A.C., Bauters, M., Boeckx, P., Alonso, J.-L.B., Zong, S., Cecco, V.D., Sitková, Z., Tielbörger, K., Brink, L. van den, Weigel, R., Homeier, J., Dahlberg, C.J., Medinets, S., Medinets, V., Boeck, H.J.D., Portillo-Estrada, M., Verryckt, L.T., Milbau, A., Daskalova, G.N., Thomas, H.J.D., Myers-Smith, I.H., Blonder, B., Stephan, J.G., Descombes, P., Zellweger, F., Frei, E.R., Heinesch, B., Andrews, C., Dick, J., Siebicke, L., Rocha, A., Senior, R.A., Rixen, C., Jimenez, J.J., Boike, J., Pauchard, A., Scholten, T., Scheffers, B., Klinges, D., Basham, E.W., Zhang, J., Zhang, Z., Géron, C., Fazlioglu, F., Candan, O., Bravo, J.S., Hrbacek, F., Laska, K., Cremonese, E., Haase, P., Moyano, F.E., Rossi, C., Nijs, I., 2020. SoilTemp: A global database of near-surface temperature. Global Change Biology 26, 6616–6629. https://doi.org/10.1111/gcb.15123

Lenoir, J., Gril, E., Durrieu, S., Horen, H., Laslier, M., Lembrechts, J.J., Zellweger, F., Alleaume, S., Brasseur, B., Buridant, J., Dayal, K., De Frenne, P., Gallet-Moron, E., Marrec, R., Meeussen, C., Rocchini, D., Van Meerbeek, K., Decocq, G., 2022. Unveil the unseen: Using LiDAR to capture time-lag dynamics in the herbaceous layer of European temperate forests. Journal of Ecology 110, 282–300. https://doi.org/10.1111/1365-2745.13837

Lenoir, J., Hattab, T., Pierre, G., 2017. Climatic microrefugia under anthropogenic climate change: implications for species redistribution. Ecography 40, 253–266. https://doi.org/10.1111/ecog.02788

Lim, K., Treitz, P., Wulder, M., St-Onge, B., Flood, M., 2003. LiDAR remote sensing of forest structure. Progress in Physical Geography: Earth and Environment 27, 88–106. https://doi.org/10.1191/0309133303pp360ra

Lüdecke, D., 2021. sjPlot: Data Visualization for Statistics in Social Science.

Lüdecke, D., 2018. ggeffects: Tidy Data Frames of Marginal Effects from Regression Models. Journal of Open Source Software 3, 772. https://doi.org/10.21105/joss.00772

Maclean, I.M.D., Duffy, J.P., Haesen, S., Govaert, S., De Frenne, P., Vanneste, T., Lenoir, J., Lembrechts, J.J., Rhodes, M.W., Meerbeek, K.V., 2021. On the measurement of microclimate. Methods in Ecology and Evolution 12, 1397–1410. https://doi.org/10.1111/2041-210X.13627

Marsh, C.D., Hill, R.A., Nowak, M.G., Hankinson, E., Abdullah, A., Gillingham, P., Korstjens, A.H., 2022. Measuring and modelling microclimatic air temperature in a historically degraded tropical forest. Int J Biometeorol. https://doi.org/10.1007/s00484-022-02276-4

McLaughlin, B.C., Ackerly, D.D., Klos, P.Z., Natali, J., Dawson, T.E., Thompson, S.E., 2017. Hydrologic refugia, plants, and climate change. Global Change Biology 23, 2941–2961. https://doi.org/10.1111/gcb.13629

Meeussen, C., De Pauw, K., Sanczuk, P., Brunet, J., Cousins, S. a. O., Gasperini, C., Hedwall, P.-O., Iacopetti, G., Lenoir, J., Plue, J., Selvi, F., Spicher, F., Uria Diez, J., Verheyen, K., Vangansbeke, P., De Frenne, P., 2022. Initial oak regeneration responses to experimental warming along microclimatic and macroclimatic gradients. Plant Biology 24, 745–757. https://doi.org/10.1111/plb.13412

Meeussen, C., Govaert, S., Vanneste, T., Bollmann, K., Brunet, J., Calders, K., Cousins, S.A.O., De Pauw, K., Diekmann, M., Gasperini, C., Hedwall, P.-O., Hylander, K., Iacopetti, G., Lenoir, J., Lindmo, S., Orczewska, A., Ponette, Q., Plue, J., Sanczuk, P., Selvi, F., Spicher, F., Verbeeck, H., Zellweger, F., Verheyen, K., Vangansbeke, P., De Frenne, P., 2021. Microclimatic edge-to-interior gradients of European deciduous forests. Agricultural and Forest Meteorology 311, 108699. https://doi.org/10.1016/j.agrformet.2021.108699

Milanesi, P., Holderegger, R., Bollmann, K., Gugerli, F., Zellweger, F., 2017. Three-dimensional habitat structure and landscape genetics: a step forward in estimating functional connectivity. Ecology 98, 393–402. https://doi.org/10.1002/ecy.1645

Miller, B.D., Carter, K.R., Reed, S.C., Wood, T.E., Cavaleri, M.A., 2021. Only sun-lit leaves of the uppermost canopy exceed both air temperature and photosynthetic thermal optima in a wet tropical forest. Agricultural and Forest Meteorology 301–302, 108347. https://doi.org/10.1016/j.agrformet.2021.108347

Milling, C.R., Rachlow, J.L., Olsoy, P.J., Chappell, M.A., Johnson, T.R., Forbey, J.S., Shipley, L.A., Thornton, D.H., 2018. Habitat structure modifies microclimate: An approach for mapping fine-scale thermal refuge. Methods in Ecology and Evolution 9, 1648–1657. https://doi.org/10.1111/2041-210X.13008

Moudrý, V., Cord, A.F., Gábor, L., Laurin, G.V., Barták, V., Gdulová, K., Malavasi, M., Rocchini, D., Stereńczak, K., Prošek, J., Klápště, P., Wild, J., 2022. Vegetation structure derived from airborne laser scanning to assess species distribution and habitat suitability: The way forward. Diversity and Distributions n/a. https://doi.org/10.1111/ddi.13644

Muñoz-Sabater, J., Dutra, E., Agustí-Panareda, A., Albergel, C., Arduini, G., Balsamo, G., Boussetta, S., Choulga, M., Harrigan, S., Hersbach, H., Martens, B., Miralles, D.G., Piles, M., Rodríguez-Fernández, N.J., Zsoter, E., Buontempo, C., Thépaut, J.-N., 2021.

ERA5-Land: a state-of-the-art global reanalysis dataset for land applications. Earth System Science Data 13, 4349–4383. https://doi.org/10.5194/essd-13-4349-2021

Naesset, E., Jonmeister, T., 2002. Assessing Point Accuracy of DGPS Under Forest Canopy Before Data Acquisition, in the Field and After Postprocessing. Scandinavian Journal of Forest Research 17, 351–358. https://doi.org/10.1080/02827580260138099

Nelson, R., Krabill, W., MacLean, G., 1984. Determining forest canopy characteristics using airborne laser data. Remote Sensing of Environment 15, 201–212. https://doi.org/10.1016/0034-4257(84)90031-2

Pincebourde, S., Suppo, C., 2016. The Vulnerability of Tropical Ectotherms to Warming Is Modulated by the Microclimatic Heterogeneity. Integr Comp Biol 56, 85–97. https://doi.org/10.1093/icb/icw014

Randin, C.F., Ashcroft, M.B., Bolliger, J., Cavender-Bares, J., Coops, N.C., Dullinger, S., Dirnböck, T., Eckert, S., Ellis, E., Fernández, N., Giuliani, G., Guisan, A., Jetz, W., Joost, S., Karger, D., Lembrechts, J., Lenoir, J., Luoto, M., Morin, X., Price, B., Rocchini, D., Schaepman, M., Schmid, B., Verburg, P., Wilson, A., Woodcock, P., Yoccoz, N., Payne, D., 2020. Monitoring biodiversity in the Anthropocene using remote sensing in species distribution models. Remote Sensing of Environment 239, 111626. https://doi.org/10.1016/j.rse.2019.111626

Roussel, J.-R., Auty, D., Coops, N.C., Tompalski, P., Goodbody, T.R.H., Meador, A.S., Bourdon, J.-F., de Boissieu, F., Achim, A., 2020. lidR: An R package for analysis of Airborne Laser Scanning (ALS) data. Remote Sensing of Environment 251, 112061. https://doi.org/10.1016/j.rse.2020.112061

Scheffers, B.R., Edwards, D.P., Diesmos, A., Williams, S.E., Evans, T.A., 2014. Microhabitats reduce animal's exposure to climate extremes. Global Change Biology 20, 495–503. https://doi.org/10.1111/gcb.12439

Sheather, S., 2009. A Modern Approach to Regression with R. Springer Science & Business Media.

Smith-Tripp, S.M., Eskelson, B.N.I., Coops, N.C., Schwartz, N.B., 2022. Canopy height impacts on the growing season and monthly microclimate in a burned forest of British Columbia, Canada. Agricultural and Forest Meteorology 323, 109067. https://doi.org/10.1016/j.agrformet.2022.109067

Stickley, S.F., Fraterrigo, J.M., 2023. Microclimate species distribution models estimate lower levels of climate-related habitat loss for salamanders. Journal for Nature Conservation 126333. https://doi.org/10.1016/j.jnc.2023.126333

Stickley, S.F., Fraterrigo, J.M., 2021. Understory vegetation contributes to microclimatic buffering of near-surface temperatures in temperate deciduous forests. Landscape Ecol. https://doi.org/10.1007/s10980-021-01195-w

Terando, A.J., Youngsteadt, E., Meineke, E.K., Prado, S.G., 2017. Ad hoc instrumentation methods in ecological studies produce highly biased temperature measurements. Ecology and Evolution 7, 9890–9904. https://doi.org/10.1002/ece3.3499

Tymen, B., Vincent, G., Courtois, E.A., Heurtebize, J., Dauzat, J., Marechaux, I., Chave, J., 2017. Quantifying micro-environmental variation in tropical rainforest understory at landscape scale by combining airborne LiDAR scanning and a sensor network. Annals of Forest Science 74, 32. https://doi.org/10.1007/s13595-017-0628-z

Valbuena, R., O'Connor, B., Zellweger, F., Simonson, W., Vihervaara, P., Maltamo, M., Silva, C.A., Almeida, D.R.A., Danks, F., Morsdorf, F., Chirici, G., Lucas, R., Coomes, D.A., Coops, N.C., 2020. Standardizing Ecosystem Morphological Traits from 3D Information Sources. Trends in Ecology & Evolution. https://doi.org/10.1016/j.tree.2020.03.006

van Ewijk, K.Y., Treitz, P.M., Scott, N.A., 2011. Characterizing Forest Succession in Central Ontario using Lidar-derived Indices. Photogrammetric Engineering & Remote Sensing 77, 261–269. https://doi.org/10.14358/PERS.77.3.261

van Leeuwen, M., Nieuwenhuis, M., 2010. Retrieval of forest structural parameters using LiDAR remote sensing. Eur J Forest Res 129, 749–770. https://doi.org/10.1007/s10342-010-0381-4

Vincent, G., Dauzat, J., Antin, C., Grau, E., Durrieu, S., 2015. Mapping plant area index of tropical forest by Lidar: calibrating ALS with TLS. Presented at the SilviLaser 2015, p. 146.

von Arx, G., Pannatier, E.G. Thimonier, A., Rebetez, M., 2013. Microclimate in forests with varying leaf area index and soil moisture: potential implications for seedling establishment in a changing climate. Journal of Ecology 101, 1201–1213. https://doi.org/10.1111/1365-2745.12121

Wickham, H., Averick, M., Bryan, J., Chang, W., McGowan, L.D., François, R., Grolemund, G., Hayes, A., Henry, L., Hester, J., Kuhn, M., Pedersen, T.L., Miller, E., Bache, S.M., Müller, K., Ooms, J., Robinson, D., Seidel, D.P., Spinu, V., Takahashi, K., Vaughan, D., Wilke, C., Woo, K., Yutani, H., 2019. Welcome to the Tidyverse. Journal of Open Source Software 4, 1686. https://doi.org/10.21105/joss.01686

Williamson, J., Slade, E.M., Luke, S.H., Swinfield, T., Chung, A.Y.C., Coomes, D.A., Heroin, H., Jucker, T., Lewis, O.T., Vairappan, C.S., Rossiter, S.J., Struebig, M.J., 2021. Riparian buffers act as microclimatic refugia in oil palm landscapes. Journal of Applied Ecology 58, 431–442. https://doi.org/10.1111/1365-2664.13784

Woods, H.A., Pincebourde, S., Dillon, M.E., Terblanche, J.S., 2021. Extended phenotypes: buffers or amplifiers of climate change? Trends in Ecology & Evolution 36, 889–898. https://doi.org/10.1016/j.tree.2021.05.010

Zellweger, F., Coomes, D., Lenoir, J., Depauw, L., Maes, S.L., Wulf, M., Kirby, K.J., Brunet, J., Kopecký, M., Máliš, F., Schmidt, W., Heinrichs, S., Ouden, J. den, Jaroszewicz, B., Buyse, G., Spicher, F., Verheyen, K., De Frenne, P., 2019a. Seasonal drivers of understorey temperature buffering in temperate deciduous forests across Europe. Global Ecology and Biogeography 28, 1774–1786. https://doi.org/10.1111/geb.12991

Zellweger, F., De Frenne, P., Lenoir, J., Rocchini, D., Coomes, D., 2019b. Advances in Microclimate Ecology Arising from Remote Sensing. Trends in Ecology & Evolution 34, 327–341. https://doi.org/10.1016/j.tree.2018.12.012

Zellweger, F., De Frenne, P., Lenoir, J., Vangansbeke, P., Verheyen, K., Bernhardt-Römermann, M., Baeten, L., Hédl, R., Berki, I., Brunet, J., Calster, H.V., Chudomelová, M., Decocq, G., Dirnböck, T., Durak, T., Heinken, T., Jaroszewicz, B., Kopecký, M., Máliš, F., Macek, M., Malicki, M., Naaf, T., Nagel, T.A., Ortmann-Ajkai, A., Petřík, P., Pielech, R., Reczyńska, K., Schmidt, W., Standovár, T., Świerkosz, K., Teleki, B., Vild, O., Wulf, M., Coomes, D., 2020. Forest microclimate dynamics drive plant responses to warming. Science 368, 772–775. https://doi.org/10.1126/science.aba6880